

Article

Trajectory Tracking of a Tri-Rotor Aerial Vehicle Using an MRAC-Based Robust Hybrid Control Algorithm

Zain Anwar Ali *, Daobo Wang, Muhammad Aamir and Suhaib Masroor

College of Automation Engineering, Nanjing University of Aeronautics and Astronautics, Nanjing 210016, China; dbwangpe@nuaa.edu.cn (D.W.); muaamir5@yahoo.com (M.A.); suhaibmasroor1@gmail.com (S.M.)

* Correspondence: zainanwar86@hotmail.com; Tel.: +86-130-1693-1051

Academic Editor: Michael Wing

Received: 2 November 2016; Accepted: 20 December 2016; Published: 19 January 2017

Abstract: In this paper, a novel Model Reference Adaptive Control (MRAC)-based hybrid control algorithm is presented for the trajectory tracking of a tri-rotor Unmanned Aerial Vehicle (UAV). The mathematical model of the tri-rotor is based on the Newton–Euler formula, whereas the MRAC-based hybrid controller consists of Fuzzy Proportional Integral Derivative (F-PID) and Fuzzy Proportional Derivative (F-PD) controllers. MRAC is used as the main controller for the dynamics, while the parameters of the adaptive controller are fine-tuned by the F-PD controller for the altitude control subsystem and the F-PID controller for the attitude control subsystem of the UAV. The stability of the system is ensured and proven by Lyapunov stability analysis. The proposed control algorithm is tested and verified using computer simulations for the trajectory tracking of the desired path as an input. The effectiveness of our proposed algorithm is compared with F-PID and the Fuzzy Logic Controller (FLC). Our proposed controller exhibits much less steady state error, quick error convergence in the presence of disturbance or noise, and model uncertainties.

Keywords: Model Reference Adaptive Control; Fuzzy Logic Controller (FLC); trajectory tracking; tri-rotor UAV

1. Introduction

Currently, research in the area of control engineering is focused on the field of unmanned flight body aircraft, such as helicopters, hex-rotor, quad-rotor, and tri-rotor robots, due to their variety of applications, especially in the area of defense [1–4]. Other areas include surveillance, environmental monitoring, agriculture, and media coverage. For any unmanned flight, the position and altitude of the robot can take advantage of sensor information [5,6]. This paper provides a trajectory tracking control algorithm for the tri-rotor aerial vehicle by taking advantage of vertical takeoff and landing (VTOL). The unmanned tri-rotor system is used for imaging of forest fires, accidents, surveillance, transportation, and the detection of manholes [7–11]. The full weight of the system depends on controlling the external bars, which requires high energy consumption.

The tri-rotor aerial vehicle has four input commands, Col, Lat, Lon, and Ped, for altitude, latitude, longitude, and angular control command. The nine outputs are (p, q, r) , (u, v, w) , and (φ, θ, ψ) , which are the rotational velocity, translational velocity, and Euler angles [12]. To rectify the rotor reaction that is found in yaw moments, a Brushless Direct Current (BLDC) motor is fixed to the triangular structure of the tri-rotor.

Some of the main reasons that the tri-rotor UAV is superior to the quad-rotor aerial vehicle are as follows: (i) Orientation of Unmanned Aerial Vehicle (UAV): By comparing the tri-rotor UAV with the quad-rotor UAV structure, the orientation of the quad-rotor rapidly disappears at larger distances due

to its structure being symmetrical. Moreover, by using Light-Emitting Diodes (LED), the operatives are notably confused in the daytime. Compared to quad-rotor UAV, tri-rotor UAV orientation is obvious at far longer distances; (ii) Natural Flying Dynamics: Tri-rotor UAVs are able to fly in a route that closely resembles the fixed-wing UAV. Rapid turning ability, forward flight, and increasing or decreasing the velocity in an intuitive pattern are the leading advantages. On the other hand, quad-rotor UAVs are not very intuitive; the main advantage of the tri-rotor UAV is that it resembles fixed wing aircraft dynamics during flight, while a quad-rotor behaves like a single rotor aircraft. The structure of the tri-rotor UAV allows the switching blade to enjoy not only the benefit of UAV's intuitive structure, hovering of flight, and forward flight capability, but also VTOL; (iii) Yaw angle controlling ability: The yaw control is used for the rotation of a UAV around its vertical axis. The yaw angle permits the UAV to make quicker turns as per a given reference. As compared to tri-rotor UAVs, the quad-rotor UAV yaw controlling is done by the variation of torque by using all four rotors. The tri-rotor UAV moves downward if any of the rotors decelerate, whereas accelerating the rotor makes UAV rotate. In switching blade UAVs, an advanced pivot back yaw mechanism essentially permits the back rotor to rotate laterally along the longitudinal axis. Rotating the UAV by using these forces rather than torque vectoring requires more propellers to act as an alternate for the application of force on the vertical axis. This means that the propellers operate at full capacity and the back propeller can still turn the UAV. If we maintain the orientation even in a rough, windy environment, it is efficient and easier to control: turning the back propeller into the wind counteracts its force, and the switching blade UAV could easily be operated in these types of environments, whereas a quad-rotor UAV of the same size would not fly well in the abovementioned case [13–15].

The latest unmanned tri-rotor systems are easy to use provided that they rely on the Fuzzy Proportional Integral (F-PI) control algorithm discussed in [16–19]. For the tri-rotor, the operating conditions of the system and the rotor movement coupled with the nonlinear F-PI controller is located outside (in the outer loop) of the system (the yaw heading is fast and reliable as it is hard to control the angle). To design a control algorithm for the nonlinear characteristics (noise and disturbance) of a tri-rotor, this paper presents the conditions for fuzzy algorithms with an existing PD controller. For comparative analysis, a tri-rotor Fuzzy Proportional Derivative (F-PD) computer simulation of response performance is presented in [20]. The main objective of the Model Reference Control (MRC) or pole-placement method is to find the input of the system and drive the system output by tracking the reference provided by the input model as closely as possible.

The basic theme is to equalize the system output provided by the reference system input; we can also say that the system output converges to the reference input exponentially [21–24]. A Fuzzy Logic Controller (FLC) mainly concerns the linguistic rules. The benefit of the fuzzy logic controller is that a clarification of a specific difficulty can be recognized with respect to human behavior so that it can be recognized by an operator, and their involvement can be used to design the controller's IF/THEN rules [25]. The biggest advantage of FLC is clarity as to the enlargement, estimation, and maintenance of the control system [26]. Many hybrid controller schemes were formerly applied for the stabilization, desired path tracking, and trajectory tracking of UAV, like the Model Reference Adaptive Control (MRAC) base (Proportional Integral Derivative, PID) controller in [27,28]. In [29], Mohammadi et al. use a fuzzy-based PID controller to control the attitude and altitude of a quad-rotor UAV. Regulation, Pole-Placement, and Tracking (RST) base dual controller scheme were proposed for controlling the stabilization of a tri-rotor UAV [30]. A fuzzy-based hybrid control algorithm was designed for the stabilization of tri-rotor UAVs [31]. An adaptive hybrid controller scheme was used to control the attitude and altitude of the tri-rotor UAV [32].

In this article, the performance of the MRAC-hybrid controller is compared with a fuzzy-based PID (F-PID) controller [33] and a Fuzzy logic controller (FLC) [34]. The key contributions of this article are (1) a novel MRAC-based fuzzy PD and fuzzy PID controller are designed to control the altitude and attitude movement of the aerial vehicle and remove the transient and steady state error; (2) the

proposed controller uses linear and angular velocity components, which are given as an input to the controller; and (3) the stability analysis of the rotational system is proved by Lyapunov stability theory.

The rest of the manuscript is structured as follows. The tri-rotor system model and preliminaries, as well as the system main engine, are discussed in Section 2. In Section 3, the design of the control algorithm is provided, such that the position, altitude, and rotational control of the vehicle are discussed along with the system stability proof. Section 4 presents the simulation results and discussions of the paper. Finally, Section 5 gives the conclusions of the paper.

2. The Tri-Rotor System Model and Preliminaries

The model of the tri-rotor aerial vehicle is taken from [35–37]. Tri-rotor UAV dynamics and parameters are multivariable and nonlinear in nature. The model of the system is shown in Figure 1, which depicts the three rotors of the UAV placed in a triangular frame. However, one rotor of the three is used as a tilt rotor as per the requirements, and this is used to nullify the effects of the torque reaction.

Assumption 1. The formation or arrangement of the tri-rotor aerial vehicle is well adjusted in terms of the orientation of the x , y , and z axis with respect to rotor 1, rotor 3, and rotor 2, respectively.

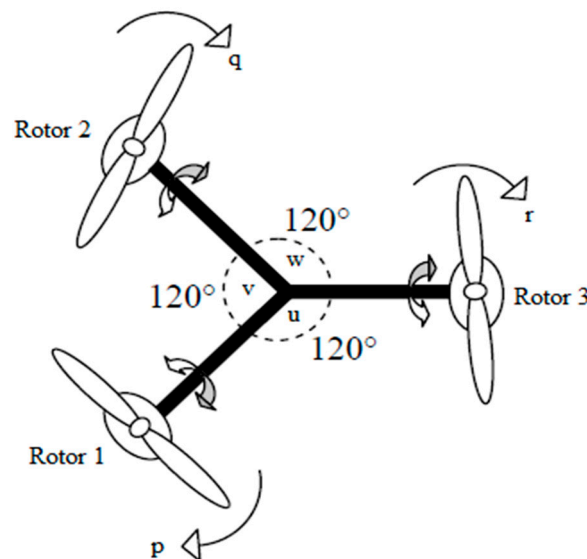


Figure 1. The structure of the tri-rotor aerial vehicle.

2.1. System Dynamics

The motor blade radius is denoted by R_T and δ_T is the total angular velocity of the system; a is the blade area, ρ_a is the air density, q should be the rotor shaft torque, t_r is the total thrust produced in the system, the aerodynamic coefficient of thrust is denoted by A_{ct} , the aerodynamic rotor shaft coefficient is A_{cq} , and A_{cp} is the aerodynamic coefficient of power.

$$A_{ct} = t_r / \rho_a a (\delta_T R_T)^2 \quad (1)$$

$$A_{cq} = q / \rho_a a (\delta_T R_T)^2 R_T \quad (2)$$

$$A_{cp} = C_p / \rho_a a (\delta_T R_T)^3 \quad (3)$$

The coefficient of power can be written as $C_p = q \delta_T$.

Hence,

$$A_{cp} = A_{cq} = q \delta_T / \rho_a a (\delta_T R_T)^3. \quad (4)$$

The total external forces and torques acting in the frame of the vehicle are given by:

$$\begin{cases} f_{ext.} = f_x + f_y + f_z \\ f_{ext.} = 0 + t_r \delta_1 |\delta_1| \sin \alpha - t_r (\delta_1 |\delta_1| \cos \alpha + \delta_2 |\delta_2| + \delta_3 |\delta_3|). \end{cases} \quad (5)$$

The tilt angle is defined by α and can be controlled by using u_4 , the yaw controller.

$$\begin{cases} \tau_{f_{ext.}} = \tau_x + \tau_y + \tau_z \\ \tau_{f_{ext.}} = \left(\begin{array}{l} \left(\frac{(3)^{0.5}}{2} * Lt_r (\delta_2 |\delta_2| - \delta_3 |\delta_3|) \right) + \left(\frac{1}{2} Lt_r (\delta_2 |\delta_2| + \delta_3 |\delta_3|) - Lt_r \delta_1 |\delta_1| \cos \alpha + k_\tau \delta_1 |\delta_1| \sin \alpha \right) \\ - (Lt_r \delta_1 |\delta_1| \sin \alpha - k_\tau \delta_1 |\delta_1| \cos \alpha \delta_2 |\delta_2| + \delta_3 |\delta_3|) \end{array} \right) \end{cases} \quad (6)$$

where f_x , f_y , and f_z are the total forces that are exerted on a body, and τ_x , τ_y , τ_z are the total torque responses along the x , y , or z direction of the Earth coordinate system.

Assumption 2. *The three-rotor UAV is rigid. Then, the nonlinear dynamics can be derived using the Newton–Euler formulas.*

For the ideal hovering and trajectory tracking coefficient of profile, drag is taken to be constant and supposed to be 0.015. The value is taken from the momentum theory [38], in which the solidity ratio is denoted by “ σ ”. To avoid all the external effects exerted on the UAV body moments, rotational and translational dynamics are used to govern the tri-rotor UAV, and are written as follows.

Translational Dynamics: We have to neglect all the effects of frame movements on the translational velocity components leading the tri-rotor aerial vehicle, which are given by:

$$\ddot{X} = (u_1/m)(\cos \varphi \cos \psi \sin \theta + \sin \psi \sin \varphi) \quad (7)$$

$$\ddot{Y} = (u_1/m)(\sin \theta \sin \psi \cos \varphi - \sin \varphi \cos \psi) \quad (8)$$

$$\ddot{Z} = -g + (u_1/m)(\cos \theta \cos \varphi). \quad (9)$$

where “ m ” is the mass, u_1 the vertical or collective is force.

Rotational Dynamics: We have to neglect the frame movements that are exerted on the body of UAV, similar to the translational velocity effects:

$$\ddot{\varphi} = qr(I_y - I_z/I_x) + (L/I_x)u_2 \quad (10)$$

$$\ddot{\theta} = pr(I_z - I_x/I_y) + (L/I_y)u_3 \quad (11)$$

$$\ddot{\psi} = pq(I_x - I_y/I_z) + (L/I_z)u_4 \quad (12)$$

where “ L ” is the length from the center of UAV, u_2 , u_3 , u_4 are the roll, pitch, and yaw control commands, respectively, generated by the propellers of the tri-rotor aerial vehicle. The inertial moments of the tri-rotor are I_x , I_y , and I_z .

Angular Rates or Euler Angles:

$$p = \dot{\varphi} - \dot{\psi} \sin \theta \quad (13)$$

$$q = \dot{\theta} \cos \varphi + \dot{\psi} \cos \theta \sin \varphi \quad (14)$$

$$r = \dot{\psi} \cos \theta \cos \varphi - \dot{\theta} \sin \varphi \quad (15)$$

The position from the center of mass in terms of the inertial frame is defined by x , y , and z , respectively. The Euler angles, φ , θ , and ψ , are used to define the position of UAV. For the trajectory tracking, neglect the higher order dynamics and let $u_1 = u_T + mg$. Consequently, $\ddot{X} = -g\varphi$, $\ddot{Y} = g\theta$, $\ddot{Z} = u_T/m$.

2.2. Main Engine (Electric Motors)

A Brushless Direct Current (BLDC) motor has a magnet on the rotor side and winding on the stator side is driven by a preset serial arrangement of the Direct Current (DC) power source called a commutator. In stator winding, back Electro Magnetic Field (EMF) is generated when the rotating magnet interacts with the stator pole. The model of BLDC motor is taken from [39].

$$E_T = Z_T I_T + \varphi \frac{dI_T}{dt} + \zeta_T \tag{16}$$

$$\zeta_T = \zeta_r \cdot \Gamma_r f(\Theta_r), \tag{17}$$

where ζ_r , Θ_r , Γ_r are the angular rotor velocity, the rotor position, and the rotor magnetic flux constant, respectively, and the generated torque is given as $\mathcal{T}_e = \frac{\zeta_T I_T}{\zeta_r}$.

In terms of machine parameters, torque is defined as:

$$\mathcal{T}_e = \mathcal{T}_L + J \frac{d\zeta_r}{dt} + \zeta \zeta_r. \tag{18}$$

3. Design of the Control Algorithm

The complete system control model is discussed in Figure 2.

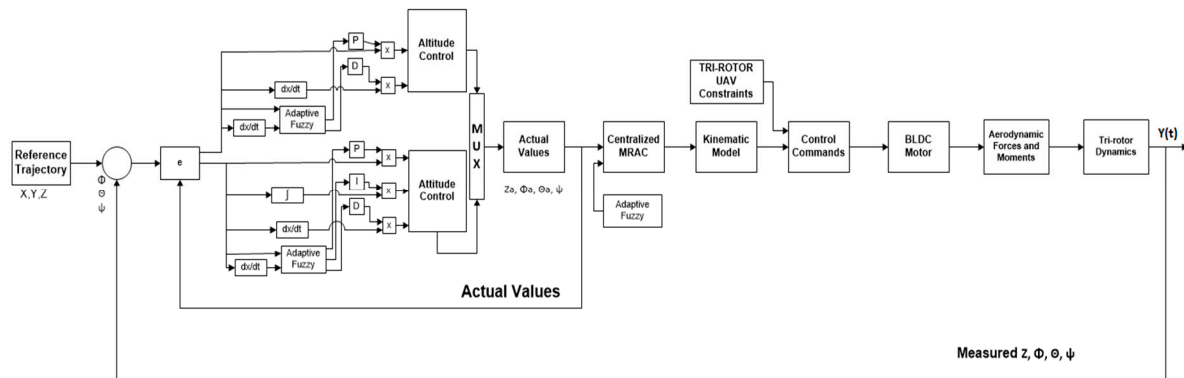


Figure 2. The block diagram of the reference trajectory control system.

3.1. The Control Objective and Its Approach

The dynamics of the UAV includes altitude, roll, and pitch and yaw control command; δ_1 , δ_2 , and δ_3 are the angular velocity of all three rotors, respectively.

Roll Control: Two conditions control the roll moment of the vehicle.

- I. Clockwise $\delta_2 < \delta_1 < \delta_3$
- II. Anticlockwise $\delta_3 < \delta_1 < \delta_2$

Pitch Control: There are also two conditions for pitch controlling.

- I. Nose-Up $\delta_1 < \delta_3 = \delta_2$
- II. Nose-Down $\delta_2 = \delta_3 < \delta_1$

Yaw Control: Yaw control has only one condition along with tilt angle.

- $\delta_3 = \delta_2 = \delta_1$ with $\alpha = 0$

Altitude Control: To achieve the preferred altitude of the UAV, the RPM of all rotors of the UAV must be the same:

- $\delta_1 = \delta_2 = \tau_{d1}$.

From translation and the rotational dynamics of UAV, the parameters u_1 , u_2 , u_3 , and u_4 are given as

$$u_1 = l_1 \tau_{c1} (\delta_1^2 - \delta_2^2) \quad (19)$$

$$u_2 = l_2 \tau_{c1} (\delta_1^2 - \delta_2^2) - l_3 \tau_{c2} \delta_3^2 \cos \alpha \quad (20)$$

$$u_3 = l_4 \tau_{d1} (-\delta_1^2 - \delta_2^2) + l_3 \tau_{d2} \delta_3^2 + l_3 \tau_{d2} \delta_3^2 \sin \alpha \quad (21)$$

$$u_4 = \tau_{c1} (\delta_1^2 + \delta_2^2) + \tau_{c2} \delta_3^2 \cos \alpha \quad (22)$$

where the thrust coefficient is τ_{c1} , τ_{c2} , and the drag coefficient is τ_{d1} , τ_{d2} .

3.2. Model Reference Adaptive Control

The MRAC algorithm is used to insure the stability of proposed system dynamics as well as the noise and time delay in the system [40]. MRAC warrants serious consideration as a means of controlling the nonlinear and adaptive system. The parameters of a controller are tuned by using the error between the reference model and close loop dynamics.

Assumption 3. The system error is written as $e_T = T_a - T_d$, where T is the x , y , or z axis, respectively.

Assumption 4. By comparing F-PID and the FLC controller, the proposed MRAC-Hybrid controller accurately follows the reference trajectory proof of their rotational system stability, as shown in Theorem 1.

3.3. Positional Control

Proposition 1. The position control of the system is written using the adaptive law for the orientation of the system by using Equations (7) and (8).

Let e_x , e_y , and e_z be the errors of speed; \dot{x}_d , \dot{y}_d , and \dot{z}_d are the desired speeds, where \dot{x}_a , \dot{y}_a , and \dot{z}_a are the actual speeds in the x , y , and z directions, respectively.

$$e_x = \dot{x}_d - \dot{x}_a \quad (23)$$

$$e_y = \dot{y}_d - \dot{y}_a \quad (24)$$

$$e_z = \dot{z}_d - \dot{z}_a \quad (25)$$

Thus, the desired roll, pitch, and yaw can be calculated by using these equations:

$$\dot{\varphi}_d = p + \dot{\psi} \sin \theta \quad (26)$$

$$\dot{\theta}_d = q - \dot{\psi} \cos \theta \sin \varphi / \cos \varphi \quad (27)$$

$$\dot{\psi}_d = r + \dot{\theta} \sin \varphi / \cos \theta \cos \varphi. \quad (28)$$

3.4. Altitude Control

From Equation (9), the altitude of UAV contains the vertical force of input u_1 and can be written as:

$$u_1 = \ddot{Z}m + gm / \cos \theta \cos \varphi, \quad (29)$$

where $\cos \theta$ and $\cos \varphi = 0$ and the fuzzy-based proportional derivative controller used to control the altitude of UAV can be expressed as:

$$FPD = -G_D \dot{z} - G_P(z_a - z_d), \tag{30}$$

where z_a is the actual and z_d is the desired altitude. The input rules for error, the derivative of error, and output rules for the fuzzy-based PD controller are shown in Figure 3, such that G_D and G_P are the proportional and derivative gains of the fuzzy controller, respectively. The output surface of the fuzzy-based proportional and fuzzy-based derivative controller are shown in Figure 4.

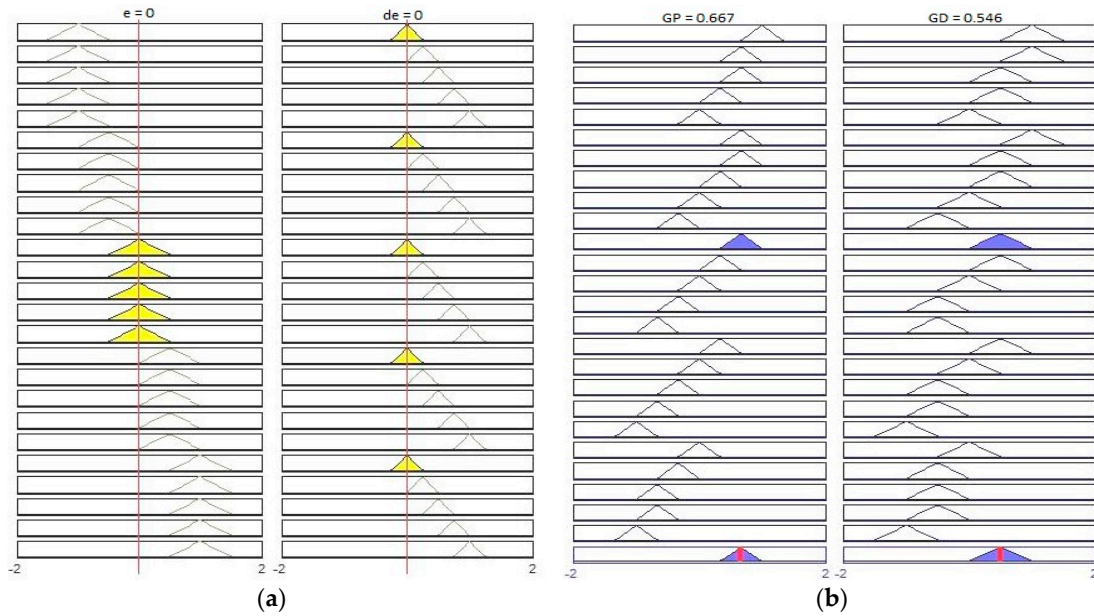


Figure 3. (a) Input rules for error and the derivative error of the fuzzy-based Proportional Derivative (PD) controller; (b) the output rules for the fuzzy-based PD controller.

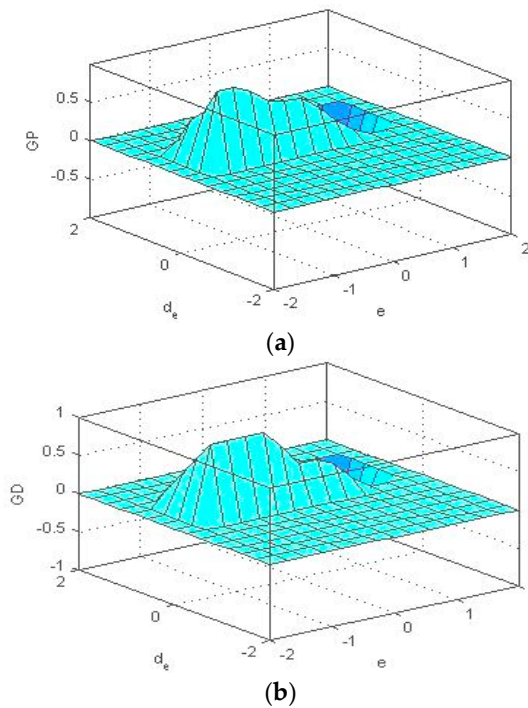


Figure 4. (a) The output surface of the fuzzy-based proportional controller; (b) the output surface of the fuzzy-based derivative controller.

3.5. Attitude Control

The fuzzy-based proportional integral derivative control method for the rotational dynamics of UAV are assigned as u_2 , u_3 , and u_4 .

Proposition 2. *The roll tracking error of UAV can be written as:*

$$e_\varphi = \varphi_a - \varphi_d. \quad (31)$$

The Lyapunov function in the system can be expressed as:

$$S_1 = G_1 e_\varphi + G_2 \int e_\varphi dt, \quad (32)$$

in which G_1 and G_2 are the gains for the fine-tuning of the system and $\int e_\varphi$ is the roll integral error. The Lyapunov stability theory is used while using the Lyapunov candidate function S_1 as a positive definite and its time derivative as a negative semi-definite, which is shown in Equation (33).

Assumption 5. *By comparing with the previous works, our proposed method provides robustness in the presence of noise and model disturbance as well as fast convergence and a zero steady state error.*

Theorem 1. *The rotational controller in the equation that is applied for the tri-rotor aerial vehicle will asymptotically converge on the rotational velocity component and tracking errors along with the model uncertainty and noise to zero.*

Proof. Consider the Lyapunov function

$$V_1 = (1/2)S_1^2. \quad (33)$$

Its derivative is

$$\dot{V}_1 = S_1 \dot{S}_1 = S_1 (G_1 \dot{\varphi}_a - G_1 \dot{\varphi}_d + G_2 e_\varphi). \quad (34)$$

Note: No control input is present in Equation (34).

If we suppose $\dot{\varphi}$ is the virtual control, the desired virtual control $(\dot{\varphi})_a$ is written as

$$(\dot{\varphi})_a = \dot{\varphi}_d - (G_2 e_\varphi / G_1) - (S_1 / G_1). \quad (35)$$

Now, the virtual control $\dot{\varphi}$ is the roll control rate of a tri-rotor along with its own error:

$$S_2 = \dot{\varphi}_a - \dot{\varphi}_d = (1/G_1)(\dot{S}_1 + S_1). \quad (36)$$

Now the amplified Lyapunov function for the second stage strategy is written as:

$$V_2 = (1/2)S_1^2 + (1/2)S_2^2. \quad (37)$$

Next we take the derivative of second step strategy:

$$\dot{V}_2 = S_1 \dot{S}_1 + S_2 \dot{S}_2. \quad (38)$$

After that, we put the values of \dot{S}_1 and \dot{S}_2 in the second step strategy into the derivative equation:

$$\dot{V}_2 = S_2 \left[e_\varphi \left(G_1^2 + \frac{G_2^2}{G_1^2} \right) + \int e_\varphi dt (G_1 G_2) + \dot{e}_\varphi \left(\frac{G_2}{G_1} \right) + q r \left(\frac{I_y - I_x}{I_x} \right) + \frac{L u_2}{I_x} - \ddot{\varphi}_d \right] - S_1 [G_1 e_\varphi + G_2 \int e_\varphi dt]. \quad (39)$$

The desired dynamics of the system can be written as

$$\dot{V}_2 = -(1/G_1)(\dot{S}_1 + S_1). \quad (40)$$

Now by putting \dot{S}_1 and S_1 in Equation (39), the desirable dynamics are given by

$$\dot{V}_2 = -\dot{e}_\varphi - e_\varphi(G_2/G_1) - \int e_\varphi dt(G_2/G_1). \quad (41)$$

The desired system dynamics verifies the negative definite of tracking error, its velocity tracking error, and integration. Now Equation (39) will be negative, if u_2 is given by

$$u_2 = -\left[e_\varphi \left(\frac{G_2}{G_1} + G_1^2 \right) + \int e_\varphi dt \left(\frac{G_2}{G_1} + G_1 G_2 \right) + \dot{e}_\varphi \left(\frac{G_2}{G_1} \right) - \ddot{\varphi}_d + qr \left(\frac{I_y - I_z}{I_x} \right) \left(\frac{I_x}{L} \right) \right]. \quad (42)$$

Similarly, the pitch control equation can be written as

$$u_3 = -\left[e_\theta \left(\frac{G_4}{G_3} + G_3^2 \right) + \int e_\theta dt \left(\frac{G_4}{G_3} + G_3 G_4 \right) + \dot{e}_\theta \left(\frac{G_4}{G_3} \right) - \ddot{\theta}_d + pr \left(\frac{I_z - I_y}{I_y} \right) \left(\frac{I_y}{L} \right) \right]. \quad (43)$$

Lastly, the yaw control equation can be written as

$$u_4 = -\left[e_\psi \left(\frac{G_6}{G_5} + G_5^2 \right) + \int e_\psi dt \left(\frac{G_6}{G_5} + G_5 G_6 \right) + \dot{e}_\psi \left(\frac{G_6}{G_5} \right) - \ddot{\psi}_d + pq \left(\frac{I_x - I_y}{I_z} \right) \left(\frac{I_z}{L} \right) \right]. \quad (44)$$

Now the fuzzy-based PID gains and roll, pitch, and yaw modules can be written as

$$FP = \frac{G_2}{G_1} + G_1^2 \quad (45)$$

$$FI = \frac{G_2}{G_1} + G_1 G_2 \quad (46)$$

$$FD = \frac{G_2}{G_1}, \quad (47)$$

where G_1 and G_2 are the gains for roll control and fuzzy rule for the PID controller, as defined after the stability performance. The input rules for error, its derivative error, and the output rules for the fuzzy-based PID controller are shown in Figure 5. The output surface of the fuzzy-based proportional, fuzzy-based derivative, and fuzzy-based integral controller are shown in Figure 6.

The roots of a characteristic equation can be obtained by placing the poles of the system at the desired location, i.e., k_a , k_b , k_c , by using the pole-placement method of Ali et al. [31]. Tuning of the system can be made faster such that the derivative of the Lyapunov candidate function becomes more negative.

$$\frac{G_2}{G_1} = k_a + k_b + k_c \quad (48)$$

$$\frac{G_2}{G_1} + G_1^2 = k_a k_b + k_a k_c + k_b k_c \quad (49)$$

$$\frac{G_2}{G_1} + G_2 G_1 = k_a k_b k_c \quad (50)$$

Proof of Stability Performance. The Lyapunov candidate function is used to insure the stability of our system. Consider the Lyapunov candidate function to be $\dot{V}_T \leq 0$, where $\forall (e_T)$ ensures the tracking error. The desired positions φ_d , θ_d , ψ_d are bounded by the supposition such that the tracking error is also bounded. Moreover, the stability is also proved by Lyapunov candidate function “V,” which is

positive and definite, and their derivative is negative. For example, $\dot{V}(e_T) < 0, \forall(e_T) \neq 0$ & $V(0) = 0, (T = \varphi, \theta, \psi)$.

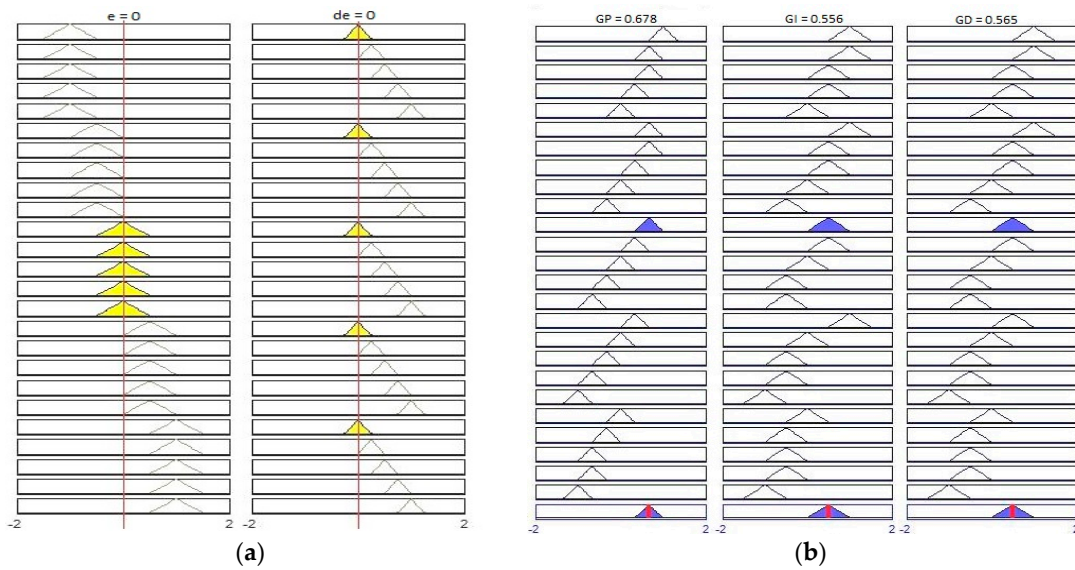


Figure 5. (a) Input rules for error and derivative error of the fuzzy-based Proportional Integral Derivative (PID) controller; (b) the output rules for the fuzzy-based PID controller.

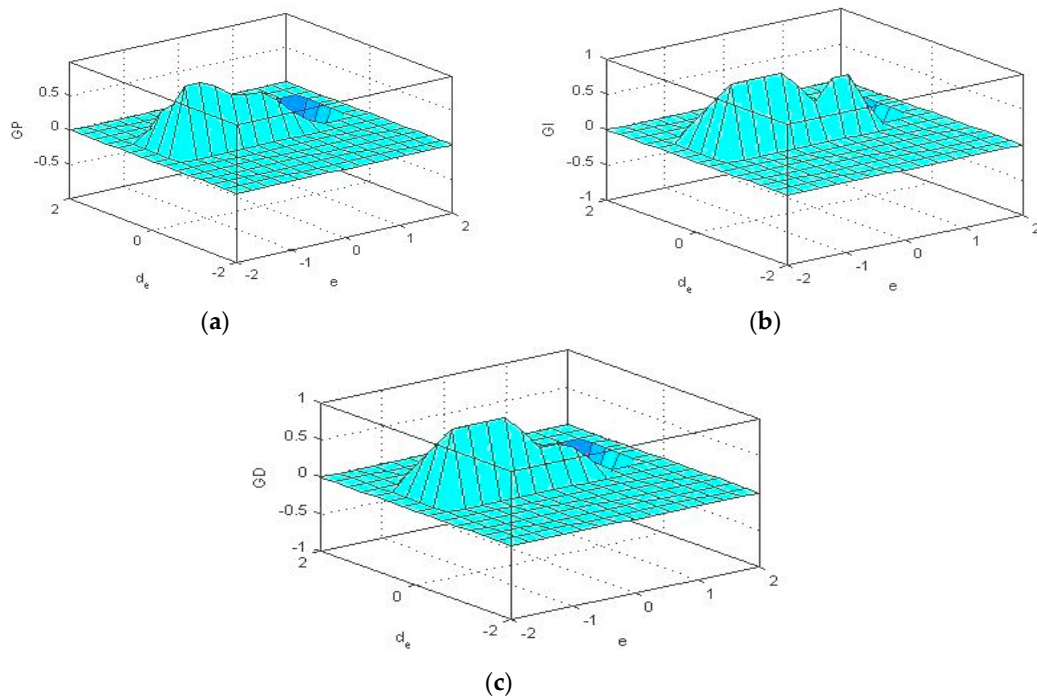


Figure 6. (a) The output surface of the fuzzy-based proportional controller; (b) the output surface of the fuzzy-based derivative controller; (c) the output surface of the fuzzy-based integral controller.

4. Simulation Results and Discussion

This section proves the effectiveness and stability of our proposed controller by using two different simulations of trajectory tracking of tri-rotor UAV. We compare our proposed MRAC-Hybrid controller with F-PID and FLC controllers by utilizing the data of [31], which are shown in Table 1.

Table 1. Tri-rotor aerial vehicle system parameters.

Parameters	Mass, m	g	L	I_x	I_y	I_z
Values	0.785	9.81	0.3050	0.3105	0.3105	0.3212
SI Units	kg	m/s ²	m	Kg·m ²	Kg·m ²	Kg·m ²

The block diagram of reference trajectories and block diagram of the desired values for the control system are shown in Figure 2. Selected trajectories using input as a reference (which constantly changes its position by using the horizontal and vertical errors of UAV) are exposed as being real applications. That will also help us to analyze the effectiveness and robustness of our proposed control algorithm in the absence of noise or disturbance in Simulation I and in the presence of noise or disturbance in Simulation Case II.

The attitude and altitude control equations are used to control the orientation of UAV, in which initial errors are controlled by the desired position of the UAV at the required altitude. The overall system performance depends on MRAC and the stability of the system is proven by Lyapunov stability.

4.1. Simulation Case I

In this case we have to simulate the inverse 2D “L” shape trajectory in the absence of random noise or disturbance, and the simulated results are presented in Figures 7–10, which show the control thrust, Euler angles and their control torque responses, vertical and horizontal flight errors, and 2D flight trajectory, respectively.

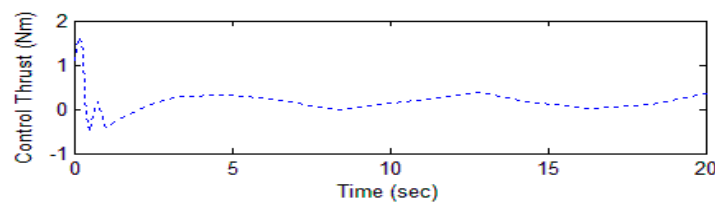


Figure 7. Control thrust of an Unmanned Aerial Vehicle (UAV) without noise or disturbance.

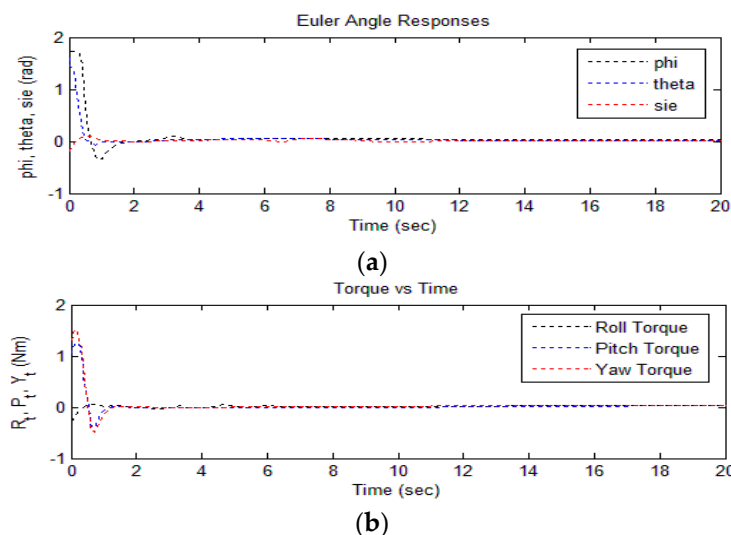


Figure 8. (a) The roll, pitch, yaw rate, and Euler angle responses of UAV; (b) torque with respect to the Euler angle response of UAV.

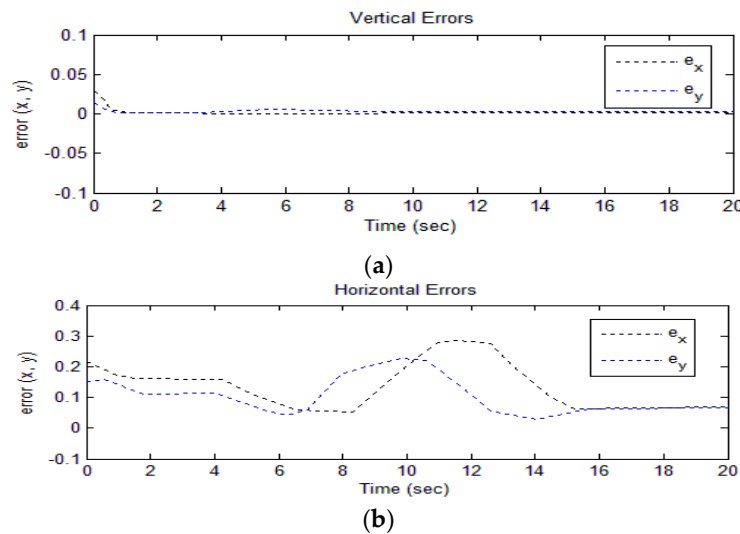


Figure 9. (a) Vertical errors of trajectory tracking in the x and y directions; (b) horizontal errors of trajectory tracking in the x and y directions.

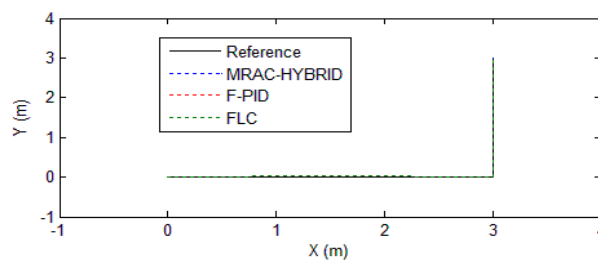


Figure 10. A 2D diagram of the real flight trajectory tracking of UAV with the reference signal, our proposed approach (the MRAC-Hybrid algorithm), the F-PID approach, and the FLC approach.

Figure 8a shows that the Euler angle responses along with their initial rates of roll, pitch, and yaw are ($\varphi = 1.8$ rad, $\theta = 1.42$ rad, $\psi = -0.2$ rad) and converge to zero at one and a half seconds. Figure 8b shows the tuning effect (control torques) of the UAV with respect to the Euler angles, with initial values of ($R_t = -0.25$ N·m, $P_t = 1.25$ N·m, $Y_t = 1.5$ N·m) and it will also nullify in a respectable amount of time. Additionally, Figure 8a,b guarantees the Euler angles tracking at the desired Euler angles in an applicable scope. The vertical trajectory tracking errors along with the initial conditions are ($e_x = 0.012$ m and $e_y = 0.025$ m), as shown in Figure 9a, and they stabilize in one second. Now the horizontal trajectory tracking errors of UAV along with the x and y directions are $e_x = 0.19$ m and $e_y = 0.15$ m, respectively, and will change with respect to time, as is shown in Figure 9b. When UAV change their movements horizontally it produces errors in their orientation, and those errors will converge to zero and stabilize the UAV using our proposed scheme.

Finally, the 2D trajectory shows that our proposed F-Hybrid controller and F-PID have better responses as compared to FLC. FLC displays a minor overshooting for a short period of time compared to both controllers. Their response is also good towards trajectory tracking, which is shown in Figure 10. In Simulation Case I, we check the robustness and effectiveness of the controllers by taking the inverse “L” shape trajectory boundary without random noise or disturbance. The trajectory equation is written as:

$$u_{x1}(t) = t_{r1}(\sin\theta_d \cos\psi_d \cos\varphi_d + \sin\psi_d \sin\varphi_d) \tag{51}$$

$$u_{y1}(t) = t_{r1}(\sin\theta_d \sin\psi_d \cos\varphi_d - \cos\psi_d \sin\varphi_d), \tag{52}$$

where “ t_{r1} ” is the total thrust, and the desired Euler angles or attitude angles can be written as

$$t_{r1} = \left(u_{x1}(t)^2 + u_{y1}(t)^2 \right)^{1/2} \tag{53}$$

$$\varphi_d = \sin^{-1} \left(\frac{u_{x1}(t) \sin \psi_d - u_{y1}(t) \cos \psi_d}{t_{r1}} \right) \tag{54}$$

$$\theta_d = \tan^{-1} \left(\frac{u_{x1}(t) \cos \psi_d + u_{y1}(t) \sin \psi_d}{u_{y1}(t)} \right). \tag{55}$$

4.2. Simulation Case II

In this case, we have to simulate the 3D trajectory of the “squared” shape in the presence of the random noise or disturbance that are present in the system; the results are shown in Figures 11–15. Figure 11 shows the random noise or disturbance in the system. Figure 12 shows the control thrust of the UAV in a noisy environment. The rest of the figures show the Euler angles, vertical and horizontal flight errors, and the 3D flight trajectory of the UAV.

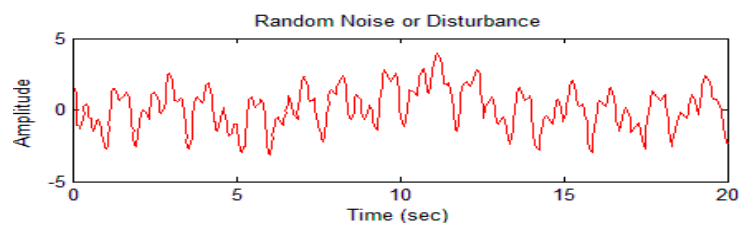


Figure 11. External noise or disturbance is added to the system dynamics.

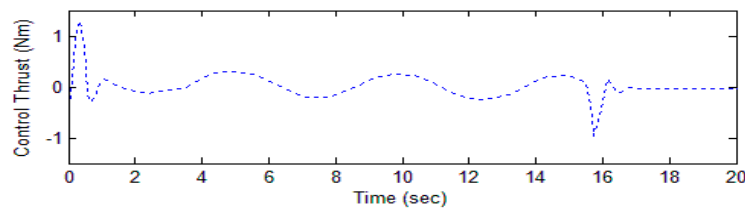


Figure 12. Control thrust of UAV under random noise or disturbance.

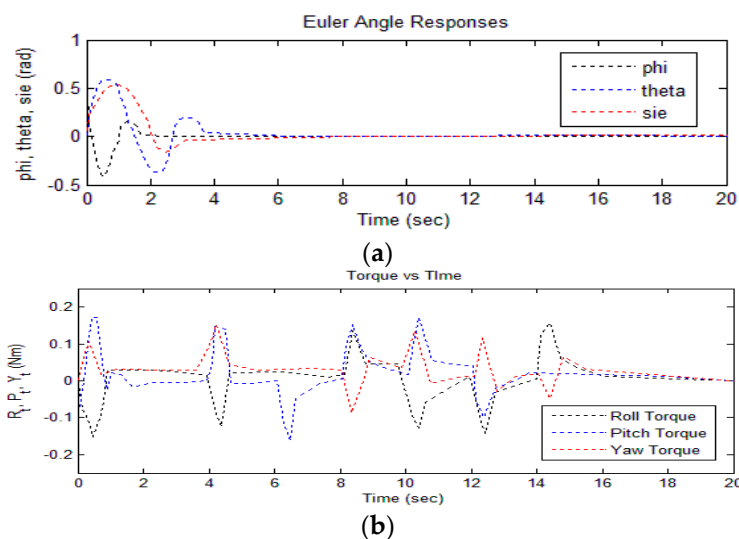


Figure 13. (a) Roll, pitch, yaw rate, and Euler angle responses of UAV; (b) torque with respect to the Euler angle responses of UAV.

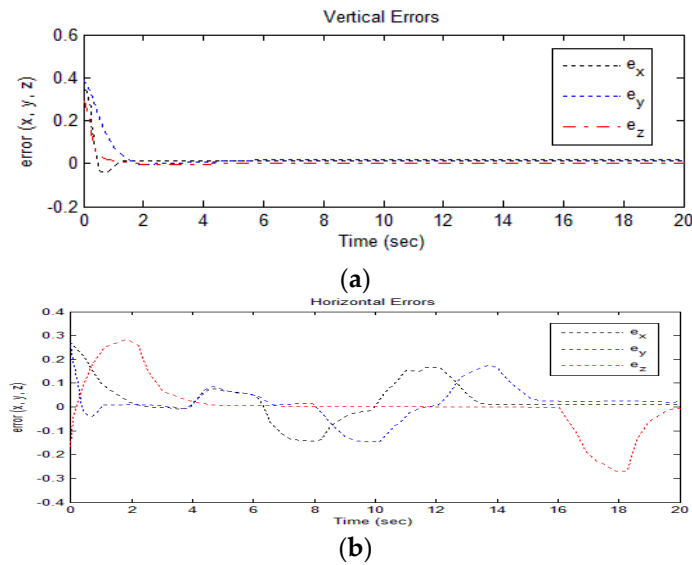


Figure 14. (a) Vertical errors of the trajectory tracking in the x , y , and z directions; (b) horizontal errors of the trajectory tracking in the x , y , and z directions.

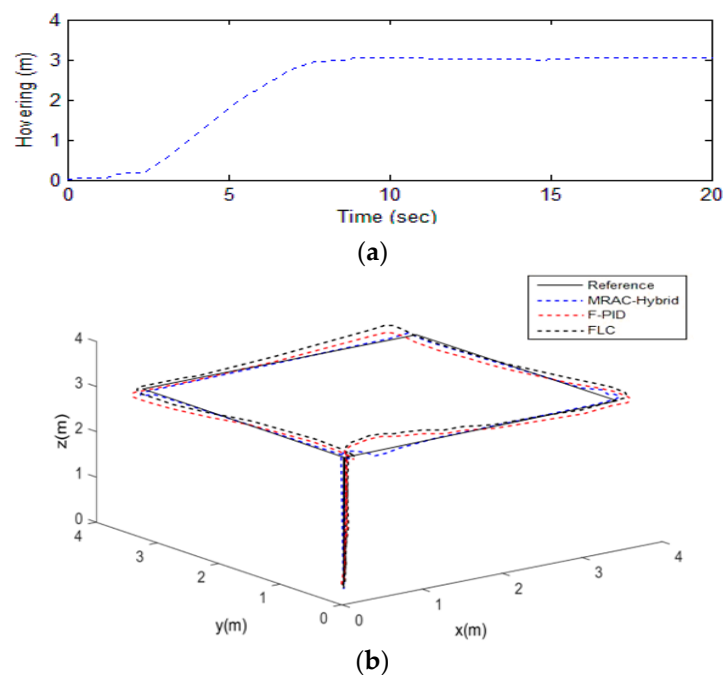


Figure 15. (a) Hovering of real flight; (b) the 3D diagram of the real flight trajectory tracking of UAV with the reference signal, our proposed approach (the Model Reference Adaptive Control (MRAC)-Hybrid algorithm), the Fuzzy Proportional Integral Derivative (F-PID) approach, and the Fuzzy Logic Controller (FLC) approach.

Figure 13a shows that the Euler angle responses along with their initial rates of roll, pitch, and yaw are ($\varphi = 0.25$ rad, $\theta = 0.30$ rad, $\psi = 0.35$ rad) and converge to zero at one and a half seconds. Figure 13b shows the turning effect (control torques) of the UAV with respect to the Euler angles, with initial values of ($R_t = -0.02$ N·m, $P_t = 0.05$ N·m, $Y_t = 0.01$ N·m) and it will also nullify in a respectable amount of time. Additionally, Figure 13a,b guarantees the Euler angles track the desired Euler angles within an applicable scope. In Figure 14a, the vertical trajectory tracking errors along with the initial conditions are ($e_x = 0.35$ m, $e_y = 0.39$ m, $e_z = 0.30$ m); they stabilize at about two seconds. In Figure 14b, the

horizontal trajectory tracking errors of UAV along the x , y , and z directions are ($e_x = 0.35$ m, $e_y = 0.28$ m, $e_z = 0.198$ m); when UAVs change their movements horizontally it produces errors in their orientation and those errors will converge to zero and stabilize the UAV using our proposed scheme. Finally, the 3D trajectory shows that our proposed F-Hybrid scheme has better steady state and transient response as compared to the previous F-PID and FLC algorithm. The rise time and settling time of velocity components, Euler angles, and control torque responses with initially little overshoot and undershoot and stabilized or converges to zero is between one and one and a half seconds.

However, if we compare the responses of our controller with an F-PID and FLC controller scheme, it will not fully converge to zero and the UAV will follow the reference trajectory along with a steady state error. In addition to this, the estimated tracking trajectory of our control algorithm is able to construct the three-rotor UAV along with aerodynamic parameters, external noises, and the parameter uncertainty of the reference path tracking the desired trajectory in an effective way, as presented in Figure 15. So, it is noticeable that our proposed control algorithm has better efficiency with disturbance and noisy environment under model uncertainties.

The effectiveness and performance of our proposed scheme are validated on the square shape bounded trajectory with noise or disturbance. The trajectory equation is written as:

$$u_{x2}(t) = t_{r2}(\sin\theta_d \cos\psi_d \cos\varphi_d + \sin\psi_d \sin\varphi_d) \quad (56)$$

$$u_{y2}(t) = t_{r2}(\sin\theta_d \sin\psi_d \cos\varphi_d - \cos\psi_d \sin\varphi_d) \quad (57)$$

$$u_{z2}(t) = t_{r2}(\cos\theta_d \cos\varphi_d), \quad (58)$$

where " t_r " is the total thrust and the desired Euler angles or attitude angles can be written as

$$t_{r2} = \left(u_{x2}(t)^2 + u_{y2}(t)^2 + u_{z2}(t)^2 \right)^{1/2} \quad (59)$$

$$\varphi_d = \sin^{-1} \left(\frac{u_{x2}(t) \sin\psi_d - u_{y2}(t) \cos\psi_d}{t_{r2}} \right) \quad (60)$$

$$\theta_d = \tan^{-1} \left(\frac{u_{x2}(t) \cos\psi_d + u_{y2}(t) \sin\psi_d}{u_{z2}(t)} \right). \quad (61)$$

5. Conclusions

This paper presented an MRAC-based hybrid control algorithm for the trajectory tracking of a tri-rotor aerial vehicle. Moreover, the control parameters of the adaptive controller are fine-tuned by the F-PD controller for the altitude control subsystem and the F-PID controller for the attitude control subsystem of the system model. Our proposed controller uses vertical and horizontal velocity errors to drive the controller. The validity of the proposed control algorithm is proven using two different computer simulations; however, in Simulation I all the controllers performed well and show a better response towards the desired tracking. Moreover, considering Simulation II, it is concluded that our proposed controller has better transient performance with no steady state error in the given trajectory under random noise or disturbance. Lastly, the proposed controller has quick convergence and robustness in the model uncertainties presented here.

Acknowledgments: This work was sponsored by the National Natural Science Foundation of China (NSFC) under Grant No. 61503185 and supported by the Key Laboratory of College of Automation Engineering, Nanjing University of Aeronautics and Astronautics, Nanjing 210016, China.

Author Contributions: The central arguments and structure of the paper were equally devised by each of the authors through a series of discussions. Zain Anwar Ali conceived the idea and carries out experimental work under the supervision of Daobo Wang. Muhammad Amir and Suhaib Masroor were involved in the writing of this research article and in the results.

Conflicts of Interest: The authors declare no conflict of interest.

References

1. Nonami, K. Prospect and recent research & development for civil use autonomous unmanned aircraft as UAV and MAV. *J. Syst. Des. Dyn.* **2007**, *1*, 120–128.
2. Langelaan, J.W.; Alley, N.; Neidhoefer, J. Wind field estimation for small unmanned aerial vehicles. *J. Guid. Control Dyn.* **2011**, *34*, 1016–1030. [[CrossRef](#)]
3. Kerns, A.J.; Shepard, D.P.; Bhatti, J.A.; Humphreys, T.E. Unmanned aircraft capture and control via GPS spoofing. *J. Field Robot.* **2014**, *31*, 617–636. [[CrossRef](#)]
4. Johnson, E.N.; Turbe, M.A. Modeling, control, and flight testing of a small-ducted fan aircraft. *J. Guid. Control Dyn.* **2006**, *29*, 769–779. [[CrossRef](#)]
5. Bracken, C.; Lyon, R.D.; Mansour, M.J.; Molnar, A.; Saulnier, A.; Thompson, S.; Sharpe, J. *Surveillance Drones: Privacy Implications of the Spread of Unmanned Aerial Vehicles (UAVs) in Canada*; Surveillance Studies Centre: Queen's University, Kingston, UK, 30 April 2014.
6. Corcoran, M. *Drone Journalism: Newsgathering Applications of Unmanned Aerial Vehicles (UAVs) in Covering Conflict, Civil Unrest and Disaster*; Australian Broadcasting Corporation: Sydney, Australia, January 2014.
7. Watts, A.C.; Ambrosia, V.G.; Hinkley, E.A. Unmanned aircraft systems in remote sensing and scientific research: Classification and considerations of use. *Remote Sens.* **2012**, *4*, 1671–1692. [[CrossRef](#)]
8. Casbeer, D.W.; Kingston, D.B.; Beard, R.W.; McLain, T.W. Cooperative forest fire surveillance using a team of small unmanned air vehicles. *Int. J. Syst. Sci.* **2006**, *37*, 351–360. [[CrossRef](#)]
9. Everaerts, J. The use of unmanned aerial vehicles (UAVs) for remote sensing and mapping. *Int. Arch. Photogramm. Remote Sens. Spat. Inf. Sci.* **2008**, *37*, 1187–1192.
10. Rango, A.; Laliberte, A.; Herrick, J.E.; winters, C.; Havstad, K.; Steele, C.; Browning, D. Unmanned aerial vehicle-based remote sensing for rangeland assessment, monitoring, and management. *J. Appl. Remote Sens.* **2009**, *3*, 033542.
11. Ali, Z.A.; Wang, D.B.; Loya, M.S. SURF and LA with RGB Vector Space Based Detection and Monitoring of Manholes with an Application to Tri-rotor UAS Images. *Int. J. Eng. Technol.* **2017**, *9*, 32–39.
12. Sane, S.P.; Dickinson, M.H. The aerodynamic effects of wing rotation and a revised quasi-steady model of flapping flight. *J. Exp. Biol.* **2002**, *205*, 1087–1096. [[PubMed](#)]
13. Sababha, B.H.; Al Zu'bi, H.M.; Rawashdeh, O.A. A rotor-tilt-free tri-copter UAV: Design, modelling, and stability control. *Int. J. Mechatron. Autom.* **2015**, *5*, 107–113. [[CrossRef](#)]
14. Ali, Z.A.; Wang, D.B.; Aamir, M. Design a robust RST controller for stabilization of a tri-copter UAV. *Pak. J. Eng. Technol. Sci.* **2016**, *5*, 60–71.
15. Kurnaz, S.; Cetin, O.; Kaynak, O. Fuzzy logic based approach to design of flight control and navigation tasks for autonomous unmanned aerial vehicles. *J. Intell. Robot. Syst.* **2009**, *54*, 229–244. [[CrossRef](#)]
16. Nho, K.; Agarwal, R.K. Automatic landing system design using fuzzy logic. *J. Guid. Control Dyn.* **2000**, *23*, 298–304. [[CrossRef](#)]
17. İrfanoğlu, B.; Alwafi, H. Attitude and Altitude Control of Two Wheeled Trirotor Hybrid Robot. *Int. J. Sci. Knowl.* **2013**, *2*, 42–56.
18. Chen, Y.-C.; Teng, C.-C. A model reference control structure using a fuzzy neural network. *Fuzzy Sets Syst.* **1995**, *73*, 291–312. [[CrossRef](#)]
19. Goodwin, G.C.; Mayne, D.Q. A parameter estimation perspective of continuous time model reference adaptive control. *Automatica* **1987**, *23*, 57–70. [[CrossRef](#)]
20. Parks, P.C. Liapunov redesign of model reference adaptive control systems. *IEEE Trans. Autom. Control* **1966**, *11*, 362–367. [[CrossRef](#)]
21. Kreisselmeier, G.; Anderson, B. Robust model reference adaptive control. *IEEE Trans. Autom. Control* **1986**, *31*, 127–133. [[CrossRef](#)]
22. Janabi, A.; Talib, H.; Sultan, L. Fuzzy Logic Controller. U.S. Patent 5,499,319, 12 March 1996.
23. Berenji, H.R. Fuzzy logic controllers. In *An Introduction to Fuzzy Logic Applications in Intelligent Systems*; Springer: New York, NY, USA, 1992; pp. 69–96.
24. Mamdani, E.H. Advances in the linguistic synthesis of fuzzy controllers. *Int. J. Man Mach. Stud.* **1976**, *8*, 669–678. [[CrossRef](#)]
25. Sugeno, M. An introductory survey of fuzzy control. *Inf. Sci.* **1985**, *36*, 59–83. [[CrossRef](#)]

26. Kim, B.S.; Calise, A.J. Nonlinear flight control using neural networks. *J. Guid. Control Dyn.* **1997**, *20*, 26–33. [[CrossRef](#)]
27. Sadeghzadeh, I.; Mehta, A.; Zhang, Y.; Rabbath, C.A. Fault-tolerant trajectory tracking control of a quadrotor helicopter using gain-scheduled PID and model reference adaptive control. In Proceedings of the Annual Conference of the Prognostics and Health Management Society, Montreal, QC, Canada, 25–29 September 2011; Volume 2.
28. Chao, H.; Cao, Y.; Chen, Y. Autopilots for small unmanned aerial vehicles: A survey. *Int. J. Control Autom. Syst.* **2010**, *8*, 36–44. [[CrossRef](#)]
29. Mohammadi, M.; Shahri, A.M. Adaptive nonlinear stabilization control for a quadrotor UAV: Theory, simulation and experimentation. *J. Intell. Robot. Syst.* **2013**, *72*, 105–122. [[CrossRef](#)]
30. Ali, Z.A.; Wang, D.B.; Javed, R.; Akbar, A. Modeling & Controlling the Dynamics of Tri-rotor UAV Using Robust RST Controller with MRAC Adaptive Algorithm. *Int. J. Control Autom.* **2016**, *9*, 61–76.
31. Ali, Z.A.; Wang, D.; Aamir, M. Fuzzy-Based Hybrid Control Algorithm for the Stabilization of a Tri-Rotor UAV. *Sensors* **2016**, *16*, 652. [[CrossRef](#)] [[PubMed](#)]
32. Ali, Z.A.; Wang, D.; Masroor, S.; Shafiq, M. Attitude and Altitude Control of Trirotor UAV by Using Adaptive Hybrid Controller. *J. Control Sci. Eng.* **2016**, *2016*, 6459891. [[CrossRef](#)]
33. Ali, Z.A.; Wang, D.; Safwan, M.; Jiang, W.; Shafiq, M. Trajectory Tracking of a Nonholonomic Wheeled Mobile Robot Using Hybrid Controller. *Int. J. Model. Optim.* **2016**, *6*, 136.
34. Sanchez, E.N.; Becerra, H.M.; Velez, C.M. Combining fuzzy, PID and regulation control for an autonomous mini-helicopter. *Inf. Sci.* **2007**, *177*, 1999–2022. [[CrossRef](#)]
35. Papachristos, C.; Tzes, A. Modeling and control simulation of an unmanned tilt tri-rotor aerial vehicle. In Proceedings of the 2012 IEEE International Conference on Industrial Technology (ICIT), Athens, Greece, 19–21 March 2012; pp. 840–845.
36. Yoo, D.W.; Oh, H.D.; Won, D.Y.; Tahk, M.J. Dynamic modeling and control system design for Tri-rotor UAV. In Proceedings of the 3rd International Symposium on Systems and Control in Aeronautics and Astronautics (ISSCAA), Harbin, China, 8–10 June 2010; pp. 762–767.
37. Yoo, D.W.; Oh, H.D.; Won, D.Y.; Tahk, M.J. Dynamic modeling and stabilization techniques for tri-rotor unmanned aerial vehicles. *Int. J. Aeronaut. Space Sci.* **2010**, *11*, 167–174. [[CrossRef](#)]
38. Peters, D.A.; Chen, S.Y. Momentum Theory, Dynamic Inflow, and the Vortex-Ring State. *J. Am. Helicopter Soc.* **1982**, *27*, 18–24. [[CrossRef](#)]
39. Moseler, O.; Isermann, R. Application of model-based fault detection to a brushless DC motor. *IEEE Trans. Ind. Electron.* **2000**, *47*, 1015–1020. [[CrossRef](#)]
40. Hosseini-Suny, K.; Momeni, H.; Janabi-Sharifi, F. Model reference adaptive control design for a teleoperation system with output prediction. *J. Intell. Robot. Syst.* **2010**, *59*, 319–339. [[CrossRef](#)]

